Investigating the Structural, Electronic and Magnetic Properties of Single Vanadium Atom Doped Germanene Monolayer using Density Functional Theory (DFT)

Usman S. L. [1], Owolabi J. A[1], Alhassan Shuaibu[2,a], and Maharaz M N[3]

[1]Department of Physics Nigerian Defence Academy, Nigeria

[2]Department of Physics Kaduna State University, Nigeria

[3]Department of Physics Federal University Dutse, Nigeria

[a]alhassan.shuaibu@kasu.edu.ng

Abstract. *In this study, density functional theory (DFT) within generalized gradient approximation (GGA) as implemented in Quantum ESPRESSO package has been employed. The structural, electronic, and magnetic properties of single Vanadium atom (V)-doped germanene monolayer have been investigated. The doping is carried out in 2x2x1 supercell with 32 atoms which gives around 3.12% doping concentration. The results revealed that single V atom doped Germanene monolayer induced both ferromagnetic and antiferromagnetic behavior with total magnetic moment of about 0.77 μB and 1.95 μB respectively. Also the behavior of the pristine germanene remains unaffected by the single V doping. The stability of the doped system are investigated by calculating cohesive and binding energies. These results are in good agreement with many reported results in case of both graphene and silicene. It's also suggested that, the single V-doped germanene monolayer can support the quantum anomalous Hall effect, which has significant potential for spintronic applications.*

Keywords: Density Functional Theory (DFT), Generalized Gradient Approximation (GGA), Structural, Electronic and Magnetic Properties, Doping, Germanene Monolayer

Introduction

Considering graphene's tremendous success as a well-known two-dimensional (2D) material [1], [2], researchers have been exploring the production of other new 2D materials using a variety of experimental techniques [3], [4]. These include phosphorene [5], [6], transition-mixed chalcogenides [7], and hexagonal boron nitride (h-BN) [8], [9]. Significant focus has been placed on 2D materials originating from heavy group-IV elements, including stanine [10], germanene [11], and silicene [12], because of their remarkable electronic characteristics.

On the other hand, germanene has demonstrated special features like enhanced thermoelectric characteristics [13], topological superconductivity, and a large-gap quantum spin Hall (QSH) effect [14]. Theoretical studies indicate that this material can be chemically functionalized to exhibit the properties of a 2D tin film and a quantum spin Hall insulator with a band gap of 0.3 eV [14]. Moreover, halogenated 2D tin structures exhibit Dirac cone-like properties at the Fermi level [15]. The electrical properties of solid-state and condensed matter materials, such as graphene

and its analogs, have been the subject of intense theoretical investigation in various fields of physics.

Extensive interest has been shown in the experimental and theoretical study of graphene and its cousins, including silicene, stanene, and germanene. This enthusiasm has several causes, one of which is silicon's limitations in large-scale integration [14], [15]. This curiosity has been piqued even further by the successful introduction of novel materials made of a single sheet of graphite, such as graphene, germanene, and stanene. But a major problem with studying isolated graphene, germanene, or stanene is that they are semi-metallic due to a linear dispersion or crossover between the valence and conduction bands at the Fermi level, which leaves a zero band gap [16]. It is concerning that there is not a band gap, or space where no allowed electron states can exist, between the valence and conduction bands. Their lack of a band gap prevents them from being used in digital transistors or other similar devices, where a band gap is necessary for the device to act as an off-switch, even if these qualities make them great candidates for applications in solar cell technology [16]. As a result, there are many ways to create a band gap in these materials, including doping, functionalization, and the adsorption of other atoms or molecules on their surfaces [13]–[15]. The alternatives are numerous, but the particular atoms or molecules needed for hybridization vary depending on the goals and intended uses.

The objective of this work is to provide a thorough investigation and clarification of the quantum mechanical effects resulting from the substitutional doping of a single Vanadium atom in germanene. This work uses the most recent first-principle density functional theory (DFT) computations to investigate the possible atomic-level effects of Vanadium doping on the electrical characteristics of a single germanene layer.

Theoretical background

General Problem of the Many-body Schrödinger Equation

To perform a DFT ground state calculation, the first thing that comes into our mind is to solve the many-body Schrödinger equation

$$\hat{H} = |\Psi_n\rangle = E_n|\Psi_n\rangle, \tag{1}$$

where $|\Psi_n\rangle$ represent the eigenfunctions of the quantum system in its *n*-th excited state, and E_n is the corresponding energy. The eigenvalues and eigenvectors of Equation 1 allow an access to all time independent ground state properties of the system [17]. If the external electro-magnetic fields are not considered, then the Hamiltonian operator $\hat{H}$ is expressed as

$$\hat{H} = \hat{T}_n + \hat{T}_e + \hat{V}_{ee} + \hat{V}_{ne} + \hat{V}_{nn}. \tag{2}$$

Here $\hat{T}_n$ and $\hat{T}_e$ are the kinetic energy operators of nuclei and electrons respectively given by

$$\hat{T}_n = \sum_j^{N_{\text{nuc}}} -\frac{\hat{\nabla}_j^2}{2M_j}, \quad \text{and} \quad \hat{T}_e = \sum_i^{N_{\text{elec}}} -\frac{\hat{\nabla}_i^2}{2}, \tag{3}$$

where the electron-electron and nuclear-nuclear Coulomb repulsions are $\hat{V}_{ee}$ and $\hat{V}_{nn}$ respectively, and $\hat{V}_{ne}$ are the electron-nuclear Coulomb attraction. These interaction terms are expressed as

$$\hat{V}_{ee} = \sum_{ij'}^{N_{elec}} \frac{1}{\left|\hat{r}_i - \hat{r}_{j'}\right|}, \quad \hat{V}_{nn} = \sum_{jJ}^{N_{nuc}} \frac{Z_j Z_J}{\left|\hat{R}_j - \hat{R}_J\right|}, \quad \text{and} \quad \hat{V}_{en} = \sum_i^{N_{elec}} \sum_j^{N_{nuc}} \frac{-Z_j}{\left|\hat{r}_i - \hat{R}_j\right|}. \tag{4}$$

Here, N_{elec}, N_{nuc} are the number of electrons and nuclei, respectively, while Z_i representing the *me*-the atom electric charges whose mass is M_i. In this case and completely in the rest of this thesis unless other ways stated, we consider the Hartree atomic mass as $\hbar = m_c = e^2 = 1$. It is also good to mention that the wave functions for nuclei are not taken into account. It is known as Born-Oppenheimer approximation (BOA).

Density Functional Theory

Subsequently, the major difficulties on electronic properties after applying BOA is not explained comprehensibly, even in case of numerical evaluations, as the remaining quantum mechanical explanation of the system is influenced by the $3N$ degrees of freedom of all the valence electrons.

The major problem is greatly simplified by the most widely used methods known DFT for determining the electronic structure of both molecules and solids [18]. DFT has reduced the discretion of the N interacting electron system to the one dimensional (1D) particle equation, which travel in an effective external potential, entirely different from $\hat{V}_{ne}$ of Equation 4. This has made the description of the many-particle system theoretically to depend on $3N$ degrees of freedom, and formalized in such a way that it depends only on 3, specifically the spatial coordinates of the electron density by means of Kohn-Sham (KS) equation [19].

Kohn-Sham Equation

The key of the Kohn-Sham (KS) approach is to replace the interacting electron system with a fictitious non-interacting one. Seeking this replacement, Equation 1 is rewritten in the following form:

$$\left[-\frac{\nabla^2}{2} + v_{ext}(\mathbf{r}) + v_H[n]\ (\mathbf{r}) + v_{xc}[n](\mathbf{r})\right]\phi_i(\mathbf{r}) = \varepsilon_i \phi_i(\mathbf{r})\ , \tag{5}$$

where $\phi_i(\mathbf{r})$ are the Kohn-Sham wave functions, v_{ext} is the external potential generated by the ions, and $v_H[n]$ is the Hatree potential given by

$$v_H[n](\mathbf{r}) = \int dr'\, v(\mathbf{r}, \mathbf{r}')n(\mathbf{r}') = \int dr' \frac{1}{|\mathbf{r}-\mathbf{r}'|} n(\mathbf{r}'). \tag{6}$$

The third potential term $v_{xc}[n]$ is called exchange-correlation potential.

Electron Density $n(\mathbf{r})$

The main central quantity in DFT is the electron density. This quantity can be defined as the summation over the whole spin coordinates of the system electrons which can be express as

$$n(\mathbf{r}) = \sum |\phi_i(\mathbf{r})|^2. \tag{7}$$

The ground state density $n(\mathbf{r})$ obtained by the KS-equations should be the same as the ground state density

$$n(\mathbf{r}) = N \int d\mathbf{r_1}\, d\mathbf{r_2} \ldots\ldots d\mathbf{r_{N-1}} |\Psi_0(\mathbf{r_1}, \mathbf{r_2}, \ldots\ldots, \mathbf{r_{N-1}}, \mathbf{r})|^2. \tag{8}$$

Note that, the wave functions are independent-particle wave functions. The word wave function uses here with its usual sense. One should always keep in mind that we will always speak of non-physical KS wave functions and not real wave functions. Most of the plane wave (PW) computational codes decompose the KS wave function into an infinite sum of plane waves:

$$\phi_{n,k}(\boldsymbol{r}) = \sum_{\boldsymbol{G}} e^{i\boldsymbol{G}\cdot\boldsymbol{r}}\, c_{n,k}^{(\boldsymbol{G})} e^{i\boldsymbol{k}\cdot\boldsymbol{r}}, \tag{9}$$

with the development of the coefficients $c_{n,k}^{(k)}$ in order the sum can be evaluated numerically.

Local Density Approximation

In general principle of the calculation, the formalism of the KS is exact. Though, the exact exchange correlation energy expression for it is still not known to make the approximation of v_{xc} to be necessary. In this study, we have used both the local density approximation (LDA), and generalized gradient approximation (GGA).

LDA has been proposed by Kohn and Sham in the original paper [19] to serve as a good approximation for v_{xc} in a system by describing its properties efficiently by varying $n(\boldsymbol{r})$, as it is the case of simple metals. This condition can be expressed mathematically as

$$\frac{|\nabla n(r)|}{n(r)k_F(r)} \le 1, \tag{10}$$

with k_F representing the Fermi momentum.

However, it has been proved that LDA gives acceptable results for a certain range of systems, with some limitations as in the case of it is a bad description of absolute energy band gaps in semiconductors and insulators. It is observed that the corrections to the exchange-correlation energy due to the in similarities the electron charge density closed in a position $\boldsymbol{r}$ are ignored in LDA implementation. For this, it may at first seem surprising that LDA works reasonably not only for simple metals. This can be partially attributed to the fact that LDA gives the correct sum rule to the exchange-correlation hole [18] which is more desirable in transport property descriptions.

That is, using LDA there is a total electronic charge equal to one electron excluded from the neighbourhood of an electron positioned at $\boldsymbol{r}$. Indeed; it can also be shown that the exchange-correlation energy depends only weakly on the detailed shape of the exchange-correlation hole [18].

Normally the exchange-correlation energy can be expressed in the form of LDA as

$$E_{\mathrm{xc}}^{\mathrm{LDA}} = \int n(\boldsymbol{r})\, \varepsilon_{\mathrm{xc}}^{\mathrm{LDA}}(n(\boldsymbol{r}))d\boldsymbol{r}, \tag{11}$$

where $\varepsilon_{\mathrm{xc}}^{\mathrm{LDA}}$ is the exchange-correlation function for a homogeneous electron. One can obtain $\varepsilon_{\mathrm{xc}}^{\mathrm{LDA}}$ with a high precision for the homogeneous electron gas using Monte-Carlo simulations and many different parameterizations can be found in the literature or in the computational codes implemented.

Generalizes Gradient Approximation (GGA)

Typically (but not always) this is more accurate than the LDA. GGA greatly reduces the bond dissociation energy error, and generally improves transition-state barriers, but unlike LDA, there is no single universal form. Generally GGA exchange correlation function can be expressed as:

$$E_{xc}^{GGA}[n(\boldsymbol{r})] = \int n\ (\boldsymbol{r})\ \varepsilon_{xc}^{GGA}[n(\boldsymbol{r}), \nabla n(\boldsymbol{r})]d\boldsymbol{r}. \tag{12}$$

Similarly ε_{xc}^{GGA} is the GGA E exchange-correlation function that can be obtained using different parameterizations.

Norm-Conserving and Ultra-soft Pseudo Potentials

The solution of Equation 5 based on the potential given in Equation 6 is completely relying on the choice of external potential v_{ext}. In case of a present work both the norm-conserving pseudo potentials (NCP) and the Ultra-soft Pseudo potentials (USP) have been used during the calculations. Generally, the main motivations for the development of the pseudo potentials concept can be described in three main points:

1. Firstly, as it is well observed that within the environment of the atom the core electrons are mostly impervious, which means the chemistry of any crystal has been carried out by the valence electrons in most of the cases. Nevertheless, it has been shown in chapter three that in most of the cases (specifically in the case of our compounds) there are no explicit definitions of which are the core electrons.

2. A large number of basis functions (e.g., plane waves) are required in the atomic wave functions. This is because of the orthogonally among the orbitals of the same angular momentum, which lead to the strong oscillating structure of the atomic wave functions mainly close to the nucleus.

An application of the pseudo potentials approximation gives a chance to freeze the core electrons and make the substitution of the actual valence wave functions by smooth node less fictitious pseudo orbitals farther from the nucleus which are identical to the true ones. Thus, pseudo potentials are fictitious potentials between the ion (formed from the nucleus and the core electrons) and the valence electrons which should satisfy the following requirements:

1. It is expected that, the presence of the pseudo potentials in KS equation must give the eigenvalues which is in close agreement with the energy levels of the valence electrons of the all-electron Schrödinger equation.

2. It has to produce a smooth node less pseudo wave functions, which is a vague from the orbitals of the exact all electron outside a certain cut-off radius $\boldsymbol{r}_c$.

3. It has to be soft. This means that it requires certifying the smoothness of pseudo wave functions.
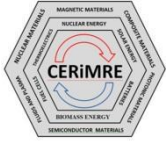
4. It also required to be finite at $r \to 0$ (regularly all pseudo potentials are also required a vanishing Laplacian at $r \to 0$ when compare with the $1/r$ divergence of the all-electron potential.

5. The conservation of the square of the norm of every valence orbital (known as norm conservation) is included up to the $r > r_c$.

6. Providing a pseudo wave function which gives equal derivative of the logarithmic with respect to the energy as the exact all-electron orbitals around the true energy eigenvalue of the orbital under consideration, similarly for $r > r_c$.

The two additional properties of NCP are clearly connected by the expression

$$\pi \left[(r\varphi) \frac{d}{dE} \frac{d}{dr} \ln \varphi_j \right]_{R,\varepsilon_j} = -2\pi \int_0^R \varphi_j^2 \, r^2 dr. \tag{13}$$

Here $R > r_c$ and j represent the eigenvalue energy that connected with the orbital j. the derivative of the logarithmic provides the properties of the scattering for the system. More significantly NCP shows similar properties of the scattering for the exact all electron orbitals close to their energy eigenvalues. This ensures a crucial quality of NCP, transferability, i. e., the good performance of the atomic pseudo potentials in different chemical environments.

For the Ultra-soft pseudo potentials (USP), the essential exit from the NCP concept is proposed by Vanderbilt and his co-workers [20]. In their method, the pseudo wavefunctions outside r_c are needed to be equal with the all-electron wavefunction, as in case of the NCP, but they are allowed to be soft as much as possible inside r_c; the constraint of the norm-conservation is completely removed to achieve this. Although some complications has been introduced, but it can significantly reduce the PW cut-off energy required during the calculations mostly, since a quite large values of r_c can be used in their approach. The main difficulties that have resulted in three:

1. First of all, since the pseudo-wave functions are equal to the all electron wave functions (and therefore have the same norm) in the interstitial, but do not have the same norm inside r_c, they are necessarily not normalized. This introduces a non-trivial overlap into the secular equation. In fact, the overlap turns out to be non-diagonal.

2. Secondly, the pseudo charge density is not obtained by computing $\sum \varphi^* \varphi$ as with NCP; among other things this would yield the wrong total charge. Rather, an augmentation term needs to be added in the core region.

3. A third, but not less important, the complication is that by relaxing the norm conservation, the resulting pseudo potentials can become less transferable.

However, Vanderbilt pseudo potentials were proposed for use in large scale calculations, for which the cost of generating pseudo potentials is negligible compared with the cost of the calculations. Accordingly, it is quite feasible to recalculate the pseudo potential as the configuration evolves during the course of the calculation.

Magnetic Properties

To determine the magnetic character of the doped system, the total (M_{Tot}) and absolute (M_{abs}) magnetizations are determined as defined, by the following expressions

$$M_{Tot} = \mu_\beta \int m(\mathrm{r})\, d\mathrm{r} \qquad M_{abs} = \mu_\beta \int |m(\mathrm{r})|\, d\mathrm{r} \tag{14}$$

Where $m(\mathrm{r}) = n^\uparrow(\mathrm{r}) - n^\downarrow(\mathrm{r})$ is the local magnetization and $n^\uparrow(\mathrm{r})/n^\downarrow(\mathrm{r})$ are the densities of spin up/down electrons. A system is labeled non-magnetic (NM) if the ground state $M_{Tot} = M_{abs} = 0$, while it is labeled ant-ferromagnetic (AFM) if $M_{Tot} \neq M_{abs}$ and $M_{Tot} < 0.1\mu_\beta$. In all other cases the system is reported as ferromagnetic (FM).

Computational Method

In this work, density functional theory (DFT) [21], [22] as implemented in Quantum ESPRESSO package [23], [24] has been use to investigate the effect of single Vanadium atom doped germanene monolayer. The exchange–correlation potential parametrized by Pardew-Burke-Ernzerhof within the generalized gradient approximation (GGA-PBE) [25], [26] has been adopted, while the ion–electron interactions are described through norm-conserving pseudopotential approach. To predict accurately the electronic properties of the doped germanene monolayer, The cut-off energy is set to 500 eV and the Brillouin zone is integrated using the Monkhorst–Pack scheme [27] of 10 × 10 × 1 and 16 × 16 × 1 for the structural stability and electronic properties calculations of the pure germanene monolayer, while 4 × 4 × 1 k-mesh of is used for the calculation of the doped system. A vacuum gap of about 15 Å along the perpendicular direction is used in other to take care of interlayer interactions. Finally, the cohesive [28] and binding [29] energy are calculated, using the following equations:

$$E_{Coh} = (E_T - n \times E_{Ge} - m \times E_V)/N \tag{15}$$

and

$$E_{bind.} = E_T - E_{Ge-vacancy} - E_V \tag{16}$$

Respectively, where E_T is the total energy of each relaxed supercell containing germanium and V atom in the supercell, E_{Ge} is the total energy of a single isolated germanium atoms, E_V is the total energy of a single isolated V atom, n and m denotes the number of Ge and V atoms respectively, $E_{Ge-vacancy}$ is the total energy of germanene supercell with one vacancy and N is the total number of atoms in a supercell.

Results and Discussion

Structural Stability

Figure 1(a)-(c), shows the optimized structures of the undoped Germanene monolayer along the given coordinates and **Figure 1(b)-(d)** shows the single V-doped Germanene monolayer along the given coordinates. In each case a clear vacuum of 15Å along the z-direction is shown. Both the structures are locally stable, exhibiting higher stability. These stable structures are characterized by planar arrangements, reflecting sp^2- and sp^3-type bonding in the undoped and

doped configurations, respectively which show that both configurations are energetically favorable, indicating that V-doping does not significantly compromise the stability of the germanene structure.
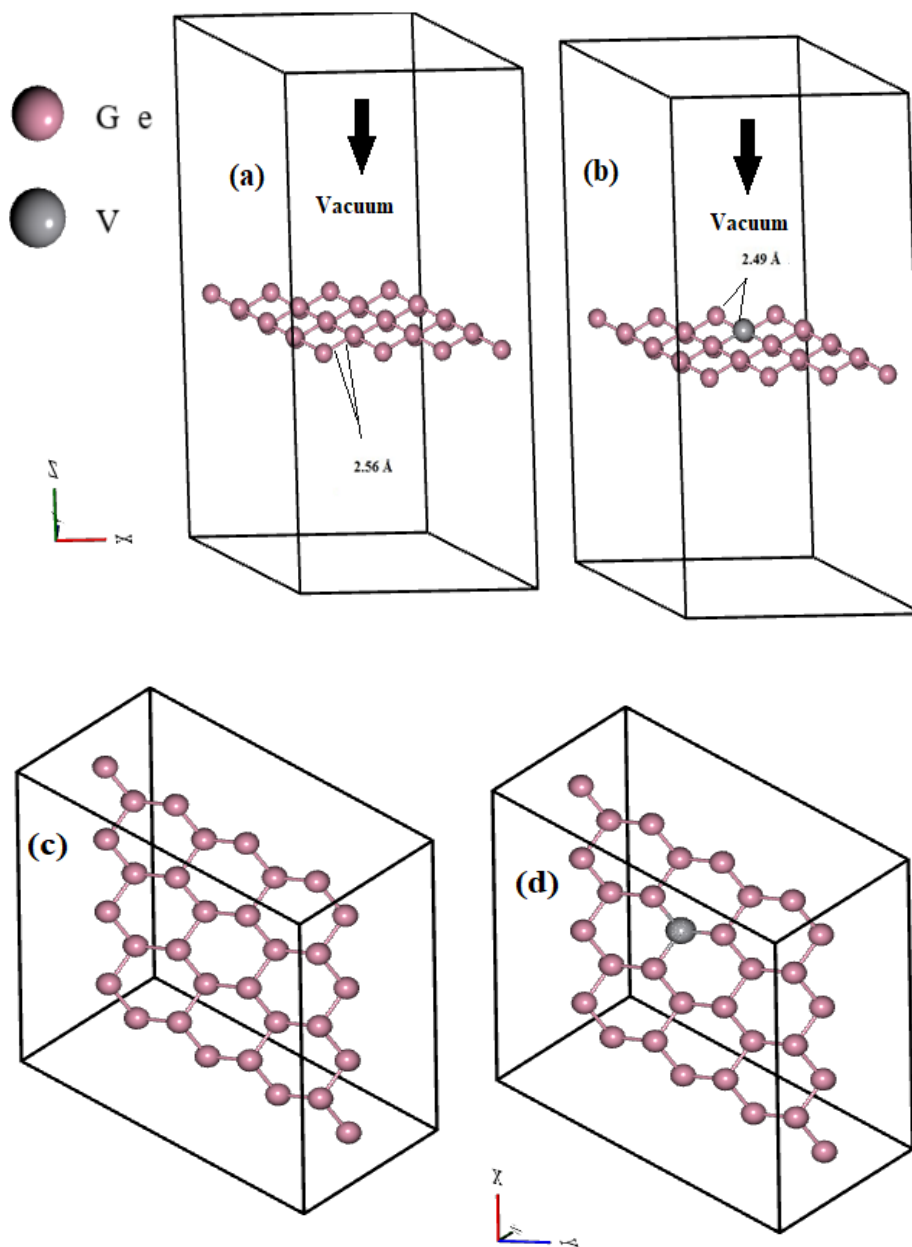

Figure 1.   Optimized model structures of (a) undoped 2 × 2 × 1 supercell of Germanene monolayer along z-axis and (b) V-doped germanene monolayer along z-axis (c) and (d) are both undoped 2 × 2 × 1 supercell of Germanene monolayer along x-y-plane and (b) V-doped germanene monolayer along x-y-plane showing the number of 32 atoms.

In other to investigate the stability of doped structures in equilibrium, E_{Coh} and $E_{bind.}$ are calculated using Eq. 1 and 2 respectively. It's found that the cohesive energy of pristine germanene sheet is found to be -4.506 eV/atom and that of V-doped system is -4.108, although these values not enough to be sure about the stability of supercells in equilibrium but still they are within range of stability, and these results are in agreement with many reported results [30]–[32]. Since binding energy is another important and necessary parameter used to understand the bond strength of each dopant. Our calculated the $E_{bind.}$ of both undoped and V-doped are -6.102 and -7.152, these results indicate that the V-doped Germane monolayer produces the localization of electrons.

Electronic Properties

The electronic properties of pure and V doped germanene monolayer were analyzed by calculating the band structure along the high-symmetry directions Γ, M, K, and Γ within the first Brillouin zone, which helps in understanding the material's electronic behavior and its energy dispersion. **Figure 2** (a) and (b) shows our calculated band structures, the results reveal that undoped germanene monolayer exhibits generic electronic characteristics, consistent with prior literature reports [33], [34]. Notably, sp³ hybridization is observed, and the p-z orbitals, oriented perpendicular to the plane, contribute to the presence of a Dirac cone at the Fermi energy, these results are in excellent agreement with reported result [34].
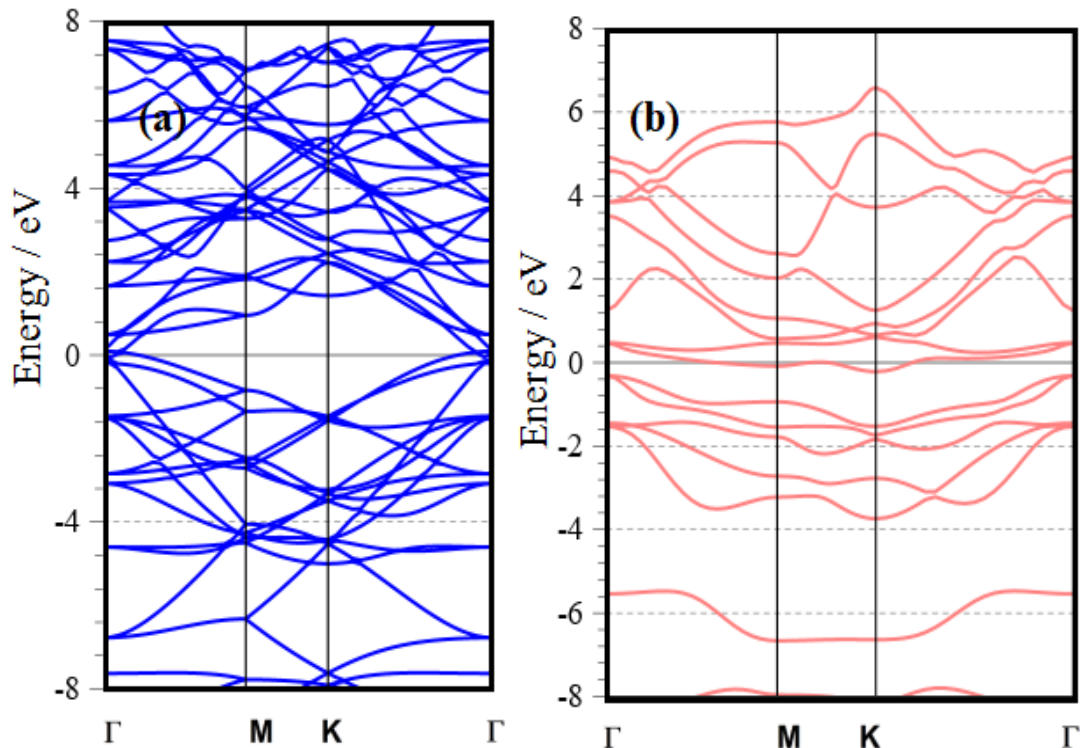

Figure 2. The calculated band structures (a) band structure of pure germanene monolayer (b) Single V-doped germanene monolayer

The unique behavior of electrons in p-z orbitals as massless fermions can be attributed to the material's buckling structure. Buckling reduces the overlap area of p-z orbitals while increasing their overlap with planar σ orbitals. Consequently, a small band gap emerges, causing a transition from linear energy dispersion at the K point to a quadratic one. The energy of the hybridized s orbital along the Γ direction is noted to be at -11 eV, while the energy of the p_z orbital falls within the range of -3 eV to -4 eV. Furthermore, the gapless energy gap exhibits along the Γ direction, showing a clear metallic and non-magnetic nature of the germanene monolayer as expected [37]. This trend illustrates that orbital energy decreases with increasing ionic radius. Importantly, these findings align closely with previously reported results.

Figure 2(b) presents our computed band structure for a single V atom-doped germanene monolayer. The graph reveals the presence of quantum anomalous Hall effect similar to the observed one in graphene and silicene [28], [29] along the K high symmetry point. This effect is expected due to the influence of the exchange field created by the presence of the V atom. This exchange field perturbs the time-reversal symmetry and induces band inversion, ultimately resulting in the realization of the anomalous Hall effect.

The success of the quantum anomalous Hall effect in this system suggests that the interaction between the V atom and its periodic image is sufficiently weak to allow the effect to persist. It's noteworthy that our doping occurs in a 2 × 2 × 1 supercell of germanene monolayer with a single V atom, representing a doping concentration of 3.12%. The distance between the V atom and its periodic images is measured at 6.12 Å. In this specific configuration, the quantum anomalous Hall Effect is not observed, likely due to the strong interaction between the V atoms, which may disrupt the effect.
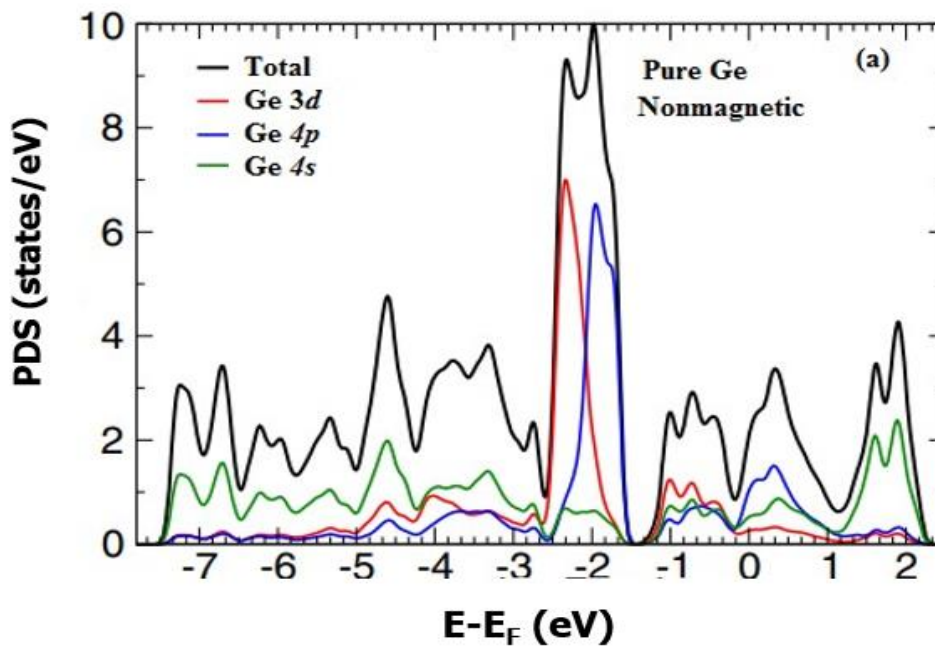

Figure 3. Calculated Total DOS and PDOS of undoped germanene monolayer

The bands near the Fermi level are a result of contributions from both the V 3d orbitals and the Germanene $4p_z$ orbitals. These orbital interactions play a crucial role in shaping the electronic properties and band structure of the doped material, as depicted in **Figure 2(a)**. Our results are in agreement with reported result [33], [34]. For more understanding on the electronic properties of the pristine monolayer a total density of state (DOS) and corresponding partial density of state (PDOS) are calculated **Figure (3)**.

The total DOS curves exhibited generic characteristics, which may be attributed to the influence of electrons in d orbitals. However, it's important to note that this study primarily considered valence electrons in the calculations, so the effect of d electrons was beyond its scope. The absence of the band gap in the Fermi level vicinity indicated that germanene possesses a semi-metallic character. The valence band, extending from zero to approximately 4 eV, is primarily composed of p_z electrons. Contributions from s electrons to the valence band become significant only at energies above roughly 2 eV. The states present at the Fermi level are predominantly attributable to p_z electrons, underscoring the metallic behavior of germanene, which is governed by these p_z electrons.

The conduction bands are primarily characterized by π* states, spanning from zero to 4 eV. Additionally, there is a mixture of states originating from σ* states. The π* and σ* bands exhibit multiple peaks, with 12 π* peaks and 10 σ* peaks discernible. The Projected Density of States (PDOS) reveals that the spin-up and spin-down DOS exhibit complete cancellation for all energy values. Consequently, pure germanene maintains its non-magnetic (NM) character, regardless of its geometry or position. This non-magnetic behavior can be attributed to the greater buckling height of germanene compared to graphene and silicene, resulting in a substantial overlap of π and σ states. In contrast, introducing vacancies may induce magnetism by disrupting the hybridization between π and σ states. This disruption occurs due to the additional energy gained through doping concentrations or absorption.

Magnetic properties

The magnetic properties of undoped single-layer germanene were investigated by examining the total and projected density of states (DOS and PDOS), as depicted in **Figure 3**. The analysis revealed the presence of hybridization between s and p orbitals at various degrees near the Fermi level. Notably, the peaks associated with these hybridized states were more pronounced than those originating from unhybridized p_z orbitals in the vicinity of the Fermi level. This suggests that electrons in undoped germanene are more localized near the Fermi level compared to their counterparts in graphene.

To explore the magnetic properties of V-doped germanene, we investigate the ferromagnetic and anti-ferromagnetic interactions between a single V atoms and first neighboring Ge atom. Our study focuses on a 2 × 2 × 1 supercell of germanene monolayer, which is considered sufficiently large to model this system effectively. This supercell contains 32 Ge atoms, with an 15 Å vacuum layer on top to minimize interactions with periodic images as shown in **Figure 1(a)** and **1(b)**.

In our investigation, we consider two configurations: ferromagnetic, as shown in **Figure 4(b)**, and anti-ferromagnetic, as depicted in **Figure 5(b)**. Both configurations involve setting the distance between a single V atom as spin up represented as V1 and the reflection as spin down represented as V2 atoms to 1.98 Å for ferromagnetic coupling and 5.69 Å for anti-ferromagnetic

coupling, followed by full relaxation of the systems. It's important to note that due to computational limitations, we do not consider paramagnetic situations in our calculations. The energy difference between the anti-ferromagnetic and ferromagnetic couplings is found to be -0.28 eV and -0.16 eV for these configurations, respectively. In the case of the ferromagnetic configuration, the interaction between the two V impurities significantly modifies the germanene sheet, as observed in **Figure 4(b)**.

From the Density of States (DOS) and Projected Density of States (PDOS) in **Figure 4(a)**, it is evident that the bands near the Fermi level are contributed to by both the 3d and 4d orbitals of Ge, with no significant contribution from V 3p and 4d orbitals. The total magnetic moment per supercell is determined to be 0.77 µB, with the primary contribution coming from V 4d states, amounting to 1.01 µB. These findings are in good agreement with those observed [33], [34].
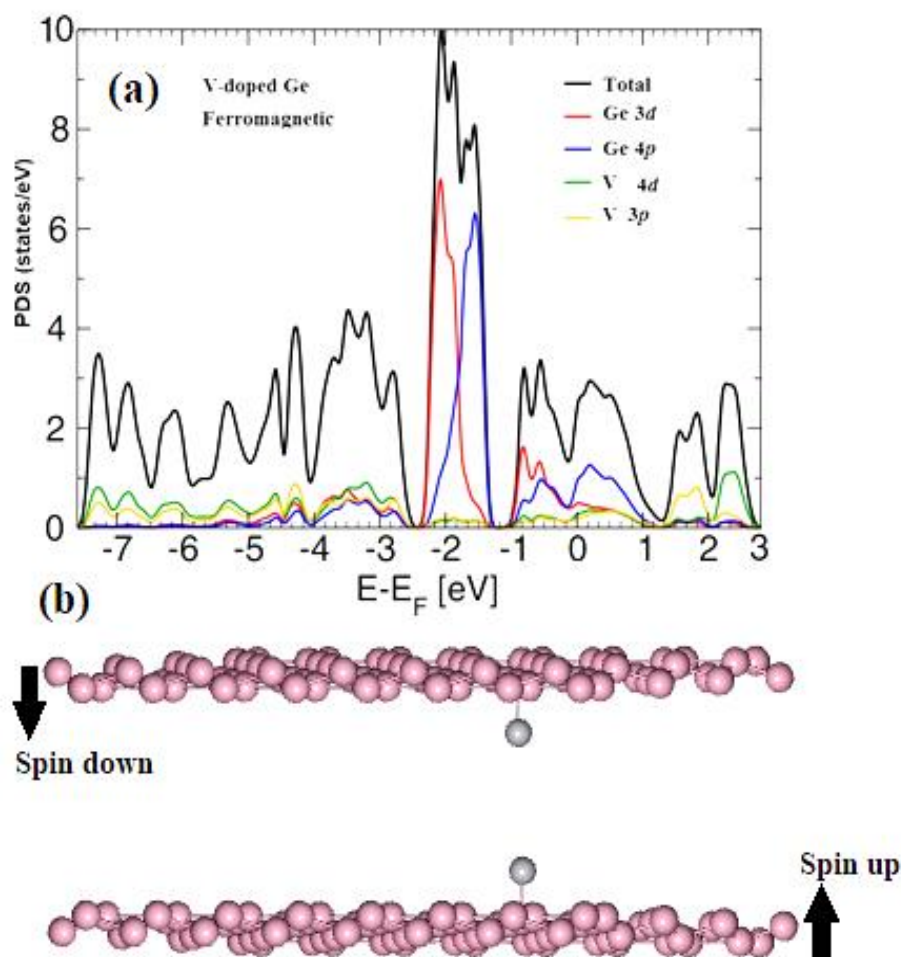

Figure 4. (a) Calculated Total DOS and PDOS of V-doped germanene monolayer and (b) geometry configuration for ferromagnetic

From the Projected Density of States (PDOS) depicted in **Figure 5(a)**, it is evident that the 3d and 4p orbitals of germanene contribute near the Fermi level, in conjunction with the 4d orbitals of V. Notably, the gap in both the p and d orbitals of germanene is significantly enhanced, reaching approximately 0.22 eV due to the interaction with the V atoms. The total magnetic moment is measured at 1.93 µB per supercell, with V 3p and V 4p contributions amounting to 1.99 µB and -0.06 µB, respectively. This value is consistent with recent reports in the literature [33], [34], [35].

However, in the case of the anti-ferromagnetic configuration shown in **Figure 5(b)**, the total magnetic moment is found to be twice that of the ferromagnetic configuration. This observation suggests that the anti-ferromagnetic coupling is energetically favored as the distance between the two V atoms increases.
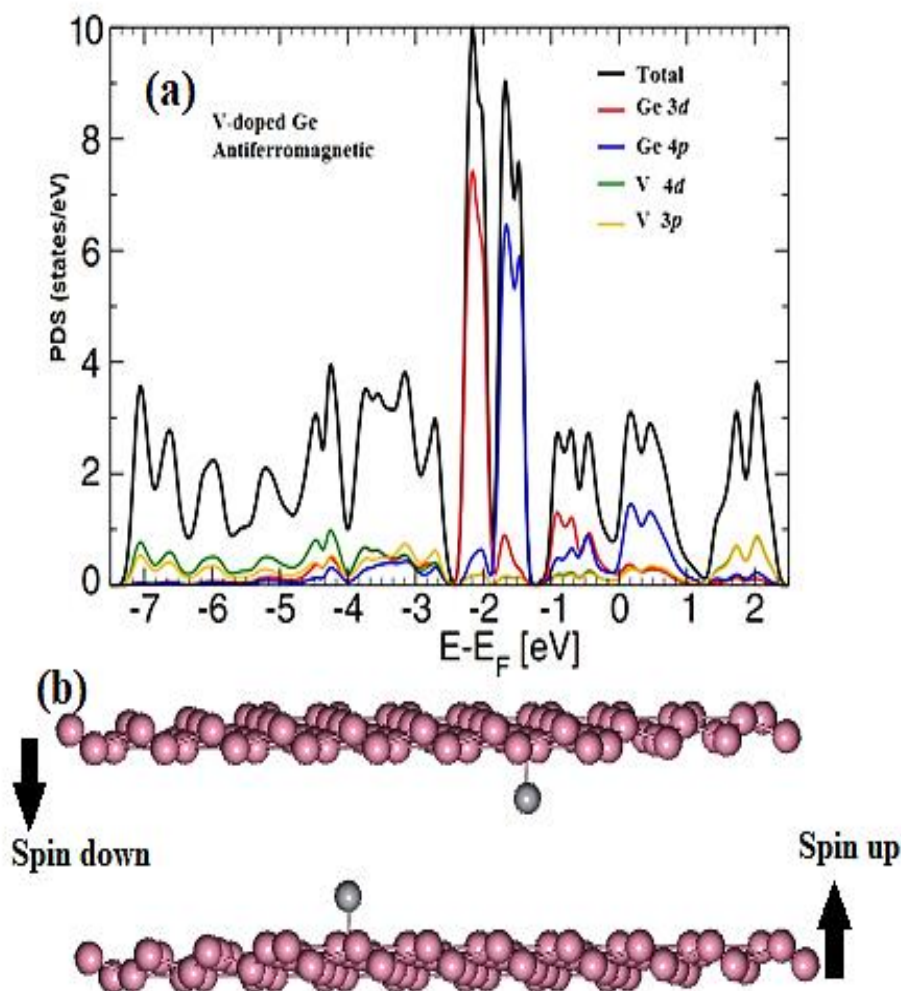

Figure 5. (a) Calculated Total DOS and PDOS of V-doped germanene monolayer and (b) geometry configuration for anti-ferromagnetic

Charge Density Contours

Figure 6 illustrates the electronic charge density of the upper valence bands for all three structural geometries under consideration. In each of these structures, the atoms exhibit a covalent bonding character. However, in the ferromagnetic geometry, as shown in **Figure 6(b)**, the covalent nature of the bonding appears to be somewhat reduced.

In both the ferromagnetic and anti-ferromagnetic geometries, the bonding between V and Ge atoms is notably weaker when compared to undoped germanene. This weakening of bonding results in a charge distribution that is concentrated more in the core region, signifying a greater degree of ionicity in these configurations [36], [37]. This observation aligns with our calculation of Poisson's ratio, which indicates a higher degree of ionic character in the anti-ferromagnetic configuration.

The variation in the intensity of electron density from the ionic core is represented by a color spectrum, with blue at the lower end and red at the higher end. The electron density is most pronounced in undoped germanene, followed by V-doped germanene, consistent with previous predictions [38]. It's worth observing that the presence of free electrons in the p_z orbital, which typically contribute to conduction in other 2D materials, is relatively low in this case due to the overlap of the sp^2 hybridized orbitals with the p_z orbitals.
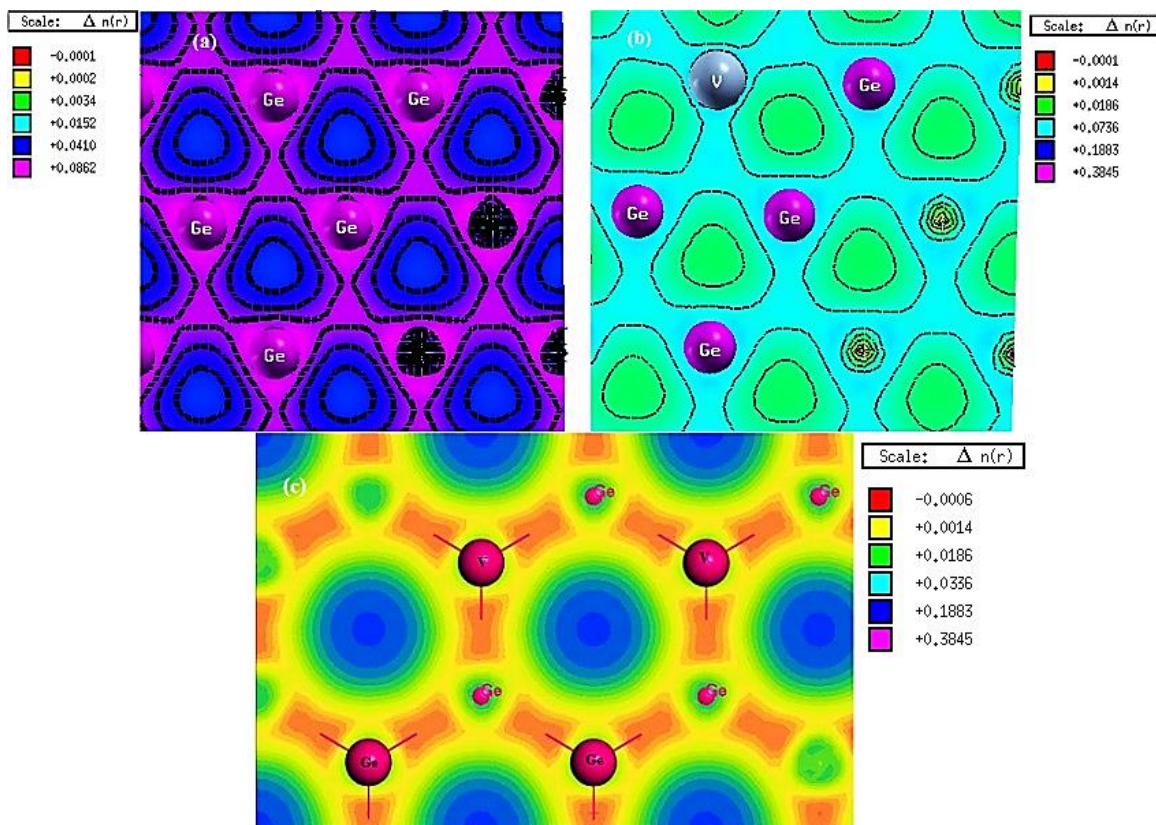

Figure 6.   Charge Density of States for upper valence band of (a) undoped germanene (b) ferro-magnetic (c) anti-ferromagnetic

Conclusions

In conclusion, this study highlights the diverse magnetic behaviors observed in V-doped germanene, with total magnetic moments ranging from 0.77 µB to 1.93 µB in different magnetic configurations. This variation can be attributed to the interaction between V impurities and the germanene lattice. The presence of a narrow electronic band gap in V-doped germanene indicates its potential as a semiconductor material. The size of the band gap can be crucial for various electronic applications. This study also suggests that V-doped germanene may host the quantum anomalous Hall effect, which has significance in the context of topological insulators and advanced electronic devices. Understanding the magnetic ordering behavior between V and Ge atoms is essential for controlling the magnetic properties of the material and tailoring it for specific applications. This research has also extended the class of two-dimensional materials beyond well-known materials like graphene and silicene, introducing V-doped germanene as a promising candidate with unique properties.

References

[1] M. Xu, T. Liang, M. Shi, and H. Chen, "Graphene-like two-dimensional materials," *Chem. Rev.*, vol. 113, no. 5, pp. 3766–3798, 2013, doi: org/10.1021/cr300263a.

[2] X. Li *et al.*, "Graphene and related two-dimensional materials: Structure-property relationships for electronics and optoelectronics," *Appl. Phys. Rev.*, vol. 4, no. 2, 2017, doi: org/10.1063/1.4983646.

[3] B. Liu and K. Zhou, "Recent progress on graphene-analogous 2D nanomaterials: Properties, modeling and applications," *Prog. Mater. Sci.*, vol. 100, pp. 99–169, 2019, doi: https://doi.org/10.1016/j.pmatsci.2018.09.004.

[4] A. Gupta, T. Sakthivel, and S. Seal, "Recent development in 2D materials beyond graphene," *Prog. Mater. Sci.*, vol. 73, pp. 44–126, 2015, doi: doi.org/10.1016/j.pmatsci.2015.02.002.

[5] M. Batmunkh, M. Bat-Erdene, and J. G. Shapter, "Phosphorene and phosphorene-based materials–prospects for future applications," *Adv. Mater.*, vol. 28, no. 39, pp. 8586–8617, 2016, doi: doi.org/10.1002/adma.201602254.

[6] A. Carvalho, M. Wang, X. Zhu, A. S. Rodin, H. Su, and A. H. Castro Neto, "Phosphorene: from theory to applications," *Nat. Rev. Mater.*, vol. 1, no. 11, pp. 1–16, 2016, doi: doi.org/10.1038/natrevmats.2016.61.

[7] S. Manzeli, D. Ovchinnikov, D. Pasquier, O. V Yazyev, and A. Kis, "2D transition metal dichalcogenides," *Nat. Rev. Mater.*, vol. 2, no. 8, pp. 1–15, 2017, doi: doi.org/10.1038/natrevmats.2017.33.

[8]   X. Wang, M. Hossain, Z. Wei, and L. Xie, "Growth of two-dimensional materials on hexagonal boron nitride (h-BN)," *Nanotechnology*, vol. 30, no. 3, p. 34003, 2018, doi: 10.1088/1361-6528/aaeb70.

[9]   A. Shuaibu, O. J. Adeyemi, and U. R. Usiekpan, "First principle study of structural, elastic and electronic properties of hexagonal boron nitride (Hex–BN) single layer," *Am. J. Condens. Matter Phys.*, vol. 9, no. 1, pp. 1–5, 2019, doi: 10.5923/j.ajcmp.20190901.01.

[10]   F. Zhu *et al.*, "Epitaxial growth of two-dimensional stanene," *Nat. Mater.*, vol. 14, no. 10, pp. 1020–1025, 2015, doi: doi.org/10.1038/nmat4384.

[11]   A. Acun *et al.*, "Germanene: the germanium analogue of graphene," *J. Phys. Condens. matter*, vol. 27, no. 44, p. 443002, 2015, doi: 10.1088/0953-8984/27/44/443002.

[12]   H. Oughaddou *et al.*, "Silicene, a promising new 2D material," *Prog. Surf. Sci.*, vol. 90, no. 1, pp. 46–83, 2015, doi: doi.org/10.1016/j.progsurf.2014.12.003.

[13]   R. Chegel, "Tunable band gap and enhanced thermoelectric performance of tetragonal Germanene under bias voltage and chemical doping," *Sci. Rep.*, vol. 13, no. 1, p. 12023, 2023, doi: doi.org/10.1038/s41598-023-39318-9.

[14]   D. Di Sante, X. Wu, M. Fink, W. Hanke, and R. Thomale, "Triplet superconductivity in the Dirac semimetal germanene on a substrate," *Phys. Rev. B*, vol. 99, no. 20, p. 201106, 2019, doi: doi.org/10.1103/PhysRevB.99.201106.

[15]   H. Qiao *et al.*, "Tunable electronic and optical properties of 2D monoelemental materials beyond graphene for promising applications," *Energy Environ. Mater.*, vol. 4, no. 4, pp. 522–543, 2021, doi: https://doi.org/10.1002/eem2.12154.

[16]   S. O. A. Ahmad *et al.*, "Application of two-dimensional materials in perovskite solar cells: recent progress, challenges, and prospective solutions," *J. Mater. Chem. C*, vol. 9, no. 40, pp. 14065–14092, 2021, doi: doi.org/10.1039/D1TC02105B.

[17]   F. A. Putra, E. Purwandari, and B. S. Nugroho, "Study of Electronic Properties of GaAs Semiconductor Using Density Functional Theory," *Comput. Exp. Res. Mater. Renew. Energy*, vol. 4, no. 2, p. 94, 2021, doi: 10.19184/cerimre.v4i2.28375.

[18]   R. O. Jones and O. Gunnarsson, "The density functional formalism, its applications and prospects," *Rev. Mod. Phys.*, vol. 61, no. 3, p. 689, 1989, doi: https://doi.org/10.1103/RevModPhys.61.689.

[19]   W. Kohn and L. J. Sham, "Self-Consistent Equations Including Exchange and Correlation Effects," *Phys. Rev.*, vol. 140, no. 4A, pp. A1133–A1138, 1965, doi: 10.1103/physrev.140.a1133.

[20]   K. Laasonen, A. Pasquarello, R. Car, C. Lee, and D. Vanderbilt, "Car-Parrinello molecular dynamics with Vanderbilt ultrasoft pseudopotentials," *Phys. Rev. B*, vol. 47, no. 16, p. 10142, 1993, doi: https://doi.org/10.1103/PhysRevB.47.10142.

[21] M. Orio, D. A. Pantazis, and F. Neese, "Density functional theory," *Photosynth. Res.*, vol. 102, pp. 443–453, 2009, doi: doi.org/10.1007/s11120-009-9404-8.

[22] P. Hohenberg and W. Kohn, "Inhomogeneous electron gas," *Phys. Rev.*, vol. 136, no. 3B, p. B864, 1964, doi: doi.org/10.1103/PhysRev.136.B864.

[23] P. Giannozzi *et al.,* "Advanced capabilities for materials modelling with Quantum ESPRESSO," *J. Phys. Condens. matter*, vol. 29, no. 46, p. 465901, 2017, doi: 10.1088/1361-648X/aa8f79.

[24] P. Giannozzi *et al.*, "QUANTUM ESPRESSO: a modular and open-source software project for quantum simulations of materials," *J. Phys. Condens. matter*, vol. 21, no. 39, p. 395502, 2009, doi: 10.1088/0953-8984/21/39/395502.

[25] J. P. Perdew, K. Burke, and M. Ernzerhof, "Perdew, burke, and ernzerhof reply," *Phys. Rev. Lett.*, vol. 80, no. 4, p. 891, 1998, doi: org/10.1103/PhysRevLett.80.891.

[26] M. Ernzerhof and G. E. Scuseria, "Assessment of the Perdew–Burke–Ernzerhof exchange-correlation functional," *J. Chem. Phys.*, vol. 110, no. 11, pp. 5029–5036, 1999, doi: org/10.1063/1.478401.

[27] R. A. Evarestov and V. P. Smirnov, "Modification of the Monkhorst-Pack special points meshes in the Brillouin zone for density functional theory and Hartree-Fock calculations," *Phys. Rev. B—Condensed Matter Mater. Phys.*, vol. 70, no. 23, p. 233101, 2004, doi: doi.org/10.1103/PhysRevB.70.233101.

[28] L. Schimka, R. Gaudoin, J. Klimeš, M. Marsman, and G. Kresse, "Lattice constants and cohesive energies of alkali, alkaline-earth, and transition metals: Random phase approximation and density functional theory results," *Phys. Rev. B—Condensed Matter Mater. Phys.*, vol. 87, no. 21, p. 214102, 2013, doi: doi.org/10.1103/PhysRevB.87.214102.

[29] M. I. Page, "Entropy, binding energy, and enzymic catalysis," *Angew. Chemie Int. Ed. English*, vol. 16, no. 7, pp. 449–459, 1977, doi: doi.org/10.1002/anie.197704491.

[30] J. He, S. Ma, P. Lyu, and P. Nachtigall, "Unusual Dirac half-metallicity with intrinsic ferromagnetism in vanadium trihalide monolayers," *J. Mater. Chem. C*, vol. 4, no. 13, pp. 2518–2526, 2016, doi: https://doi.org/10.1039/C6TC00409A.

[31] L. Liu, Y. Ji, Y. Liu, and L. Liu, "First-principle studies on the Ga and As doping of germanane monolayer," *J. Appl. Math. Phys.*, vol. 7, no. 1, pp. 46–54, 2019, doi: 10.4236/jamp.2023.1111239.

[32] X. Gong, Z. Ye, S. Lu, K. Liu, J. Liu, and Z. Liu, "Tuning the structural and electronic properties of arsenene monolayers by germanene, silicene, and stanene domain doping," *Phys. E Low-dimensional Syst. Nanostructures*, vol. 122, p. 114152, 2020, doi: doi.org/10.1016/j.physe.2020.114152.

[33] Z.-K. Yang, J.-R. Wang, and G.-Z. Liu, "Effects of Dirac cone tilt in a two-dimensional Dirac semimetal," *Phys. Rev. B*, vol. 98, no. 19, p. 195123, 2018, doi:

doi.org/10.1103/PhysRevB.98.195123.

[34]   J. E. Padilha and R. B. Pontes, "Electronic and transport properties of structural defects in monolayer germanene: an ab initio investigation," *Solid State Commun.*, vol. 225, pp. 38–43, 2016, doi: doi.org/10.1016/j.ssc.2015.10.019.

[35]   A. Ali *et al.*, "First-principles investigation on electronic structure, magnetic states and optical properties of Mn-doped SnS2 monolayer via strain engineering," *Phys. E Low-dimensional Syst. Nanostructures*, vol. 134, p. 114842, 2021.

[36]   J. C. Golden, V. Ho, and V. Lubchenko, "The chemical bond as an emergent phenomenon," *J. Chem. Phys.*, vol. 146, no. 17, 2017.

[37]   H. Wang *et al.*, "Interfacial engineering of ferromagnetism in wafer-scale van der Waals Fe4GeTe2 far above room temperature," *Nat. Commun.*, vol. 14, no. 1, p. 2483, 2023.

[38]   N. Dhar and D. Jana, "A DFT perspective analysis of optical properties of defected germanene mono-layer," *Phys. Sci. Rev.*, vol. 3, no. 7, p. 20170164, 2018.